Journal of Fundamental and Applied Sciences

ISSN 1112-9867

Available online at http://www.jfas.info

Research Article

COMPUTATIONS OF TURBULENT NON-PREMIXED COMBUSTION AND MODELING OF FLAME WALL INTERACTION

R. Renane[1*], R. Allouche[1], S. Laazab[1] , A. Nour[2]

[1]Laboratory of aeronautical sciences, institute of aeronautics and space studies, University of Blida1, Algeria

[2]Laboratory of engines dynamics and vibroacoustics, UMBB Algeria

Received: 31 October 2018 / Accepted: 25 December 2018 / Published online: 01 May 2019

ABSTRACT

The aim of this work is to simulate the thermoelastic behavior of the wall of the combustion chamber of the ALLISON-T56 turboprop under the influence of dynamic loads and turbulent diffusion flame. This work is presented in two sections: The first step is to simulate and analyze the flame structure and determine for given fuel flow and preheating temperature of fresh gas the behavior of the thermodynamic parameters of combustion. The numerical approach is based on the resolution of basic equations of turbulent combustion using Ansys-Fluent software where the turbulence model viscous-SST k-omega is chosen. In the second step, the thermoelastic behavior of the wall of the combustion chamber is simulated. The simulation results are presented and discussed in the last section.The numerical results is validated by the experimental results realized on the turboprop engine Allison-T56 test bench of Air-Algerie Company.

Keywords: Numerical simulation, Diffusion turbulent flame, Combustion chamber, Thermoelastic stress

Author Correspondence, e-mail: r.renane@yahoo.fr

doi: http://dx.doi.org/10.4314/jfas.v11i2.4

1. INTRODUCTION

Combustion is one of the means of energy conversion, characterized by a highly exothermic irreversible reaction between an oxidant and a fuel. The study of this phenomenon has a considerable interest in the aviation sector [1, 2]. The main preoccupation of manufacturers and researchers, is to master the behavior of various thermodynamic parameters for efficient and ecological combustion [3]. Our work is a contribution to the analysis and simulation of the structure of the turbulent diffusion flame in annular combustion chamber of turboprop ALLISON-T56 (Figure 1). The fuel used in our study is kerosene, which has a high calorific value of 43.15 MJ.kg-1 [8]. In this work we are interested first to the geometry of the combustion chamber studied; thereafter, we present the discretization of the computational domain by the mesh generation using the Gambit software (Figure 2). The equations governing the gaseous reactants flows are recalled in the previous section where a brief reminder of the k-e turbulence model used is presented. The simulation results are presented and discussed in the last section, and a comparison is made with the scientific literature. On the other hand, the temperature reached in the aeronautical combustion chambers exceeds the limit characteristics of thermal resistance of current materials; it's for this reason that the temperature at the end of combustion must be controlled. The thrust of the engine is directly related to the temperature of gas emissions. We conceive the importance of having materials resistant to high temperatures, which have good mechanical strength and corrosion resistance, that they can supporting overheating without the risk of weakening before high stresses (creep), and finally, to be elaborate without need for heat treatment. To analyze the interaction of the turbulent flame on the structure, the thermoelastic behavior of the wall of the combustion chamber is simulated using Ansys-Fluent code. A brief reminder is given of the thermoelastic theory developed by W.D.KINGERY [18], as well as the most used elastic limit criteria for metals. The results of this section are presented and discussed below. Finally, the transient temperature field through the wall of a cylindrical element of tubular combustion chamber will be simulated, taking into account the characterization of the thermal expansion, the thermoelastic stresses and strains with the physical properties of refractory materials. The mathematical model based on the heat equation in its general form (Transitional in three dimensions) [10], coupled with laws of thermoelastic behavior is solved using a house code, where the boundary conditions of the problem are introduced from the simulation results obtained by Ansys-Fluent software such as the initial internal temperature of the wall, as well as the data provided by the engine test bench.

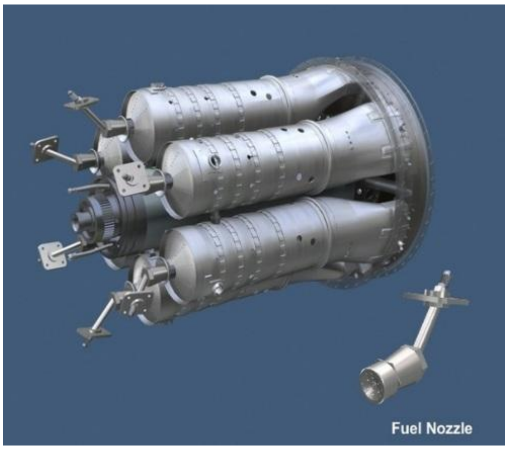

Fig.1a. Allison T56 engine combustion chamber assembly [14]

Fig.1b. T56 Gas turbine combustor liner [21]

2. MATHEMATICAL MODELS

For this study, calculations are executed by using the Ansys software, where several models of turbulence are available in this code, the models with one and two transport equations use partial derivative equations to connect the fluctuations of flow to the average sizes of variables [6]. We limit as an example to present thereafter the SST k-omega model [5-7,9]. In the second section, the Ansys-Fluent code is used again to simulate the interaction of the turbulent flame on the structure and the thermoelastic behavior of the wall of the combustion chamber; a brief reminder is given of the thermoelastic theory developed by W.D.KINGERY.

2.1 SST k-omega model

The results obtained by the model, according to Menter are very sensitive to the value of w imposed outside the boundary layer, the model SST k-w therefore represents a model alternative. It combines both models k-w and k-ε. Two equations are solved, one for the specific dissipation w and the other for the kinetic energy of turbulence k, so the equations for k and w are, more details can be given by the ref [7,9,24]:

$$\frac{\partial}{\partial t}(\bar{\rho}k)+\frac{\partial}{\partial x_j}(\bar{\rho}\tilde{u}_j k)=\bar{\rho}P-C_u\bar{\rho}\omega k+\frac{\partial}{\partial x_j}\left[(\bar{\mu}+\sigma_k\bar{\mu}_t)\frac{\partial k}{\partial x_j}\right] \quad (3.71)$$

$$\frac{\partial}{\partial t}\left(\bar{\rho}\omega\right)+\frac{\partial}{\partial x_j}\left(\bar{\rho}\tilde{u}_j\omega\right)=\frac{\gamma\bar{\rho}}{\bar{\mu}_t}P-\beta\bar{\rho}\omega^2+\frac{\partial}{\partial x_j}\left[\left(\bar{\mu}+\sigma_\omega\bar{\mu}_t\right)\frac{\partial\omega}{\partial x_j}\right]+\left(1-F_1\right)2\bar{\rho}\sigma_{\omega 2}\frac{1}{\omega}\frac{\partial k}{\partial x_j}\frac{\partial\omega}{\partial x_j} \quad (222)$$

The constants σ_k , σ_ω ,β and γ are determined from the relation [7]: $\phi = F_1\phi_1 + (1 - F_1)\phi_2$

2.2 Boundary conditions

The main boundary and initials conditions used in fluent software are obtained from reference [22,23]. The initial conditions mainly concern the parameters of air and fuel admission to the combustion chamber of Allison engine T56 are given by the table 1. These operating conditions are used in our study.

Table 1. Operating conditions during take-off with specific boundary conditions

Combustor inlet temperature [K]	566.15
Combustor inlet pressure [Pa]	923897
Total mass flow rate, m_a [kg/s]	14.154
Air/flow ratio	50
Inlet flow velocity [m/s]	30
Conduction coefficient of wall [W/m²K]	288
Turbulent intencity [%]	7
Turbulent viscosity ratio	10

Table 2. Cartesian cordinate system of flow direction at the dome holes

Holes Number	Direction of flow Cartesian coordinate system		
	X	Y	Z
N°1	-0.97	0	0.24
N°2	-0.686	-0.686	0.24
N°3	0	-0.97	0.24
N°4	0.686	-0.686	0.24
N°5	0.97	0	0.24
N°6	0.686	0.686	0.24
N°7	0	0.97	0.24
N°8	-0.686	0.686	0.24

The distribution of the mass flow of air through the different holes of a single flame tube of the combustion chamber is given in Fig.2 by ref [22,23].

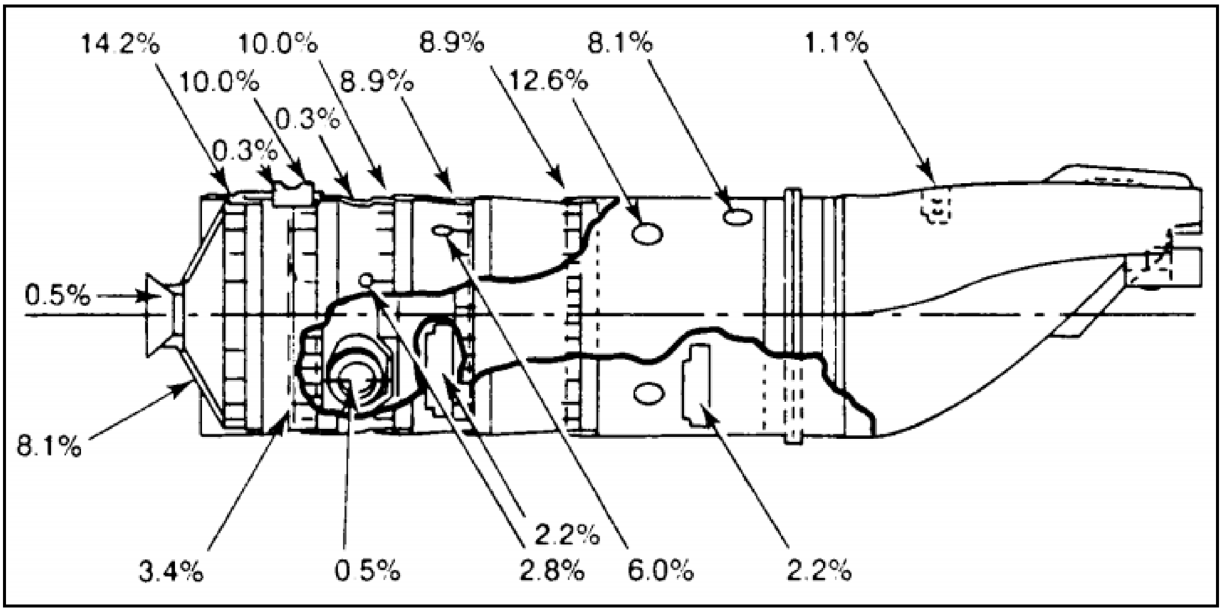

Fig.2. Airflow distribution of Allisson T56 engine combustor liner [22]

2.3 Thermoelastic approch

Developed by KINGERY [18], this approach in terms of constraints assumes a homogeneous, isotropic and elastic linear mechanical behavior [4-10-13]. In a state of biaxial stress, the thermally induced stress at the surface during instantaneous cooling is given by:

$$\sigma_{ideal} = \frac{(E.\alpha.\Delta T)}{(1-\nu)} \tag{7}$$

E: Young's modulus (MPa), α: Coefficient of thermal expansion ($° C^{-1}$), ν: Poisson's ratio and ΔT: Temperature difference (°C)

2.4. Isotropic elasticity

In the elastic case, two elastic constants are sufficient:

The Young's modulus **E** and the Poisson's coefficientν,

More precisely, the matrix of the elastic constants is written for an isotropic material [15-19]:

$$[C]=\frac{E}{(1+v)(1-2v)}\begin{bmatrix} 1-v & v & v & & 0 & \\ v & 1-v & v & & 0 & \\ v & v & 1-v & & 0 & \\ 0 & 0 & 0 & (1-2v)/2 & 0 & 0 \\ 0 & 0 & 0 & 0 & (1-2v)/2 & 0 \\ 0 & 0 & 0 & 0 & 0 & (1-2v)/2 \end{bmatrix} \quad (8)$$

The Constraint vector is given by:

$$\{\sigma\}=\begin{bmatrix}\sigma_x & \sigma_y & \sigma_z & \sigma_{yz} & \sigma_{zx} & \sigma\end{bmatrix}^T \quad (9)$$

The elastic deformation vector is given by:

$$\{\varepsilon_{el}\}=\begin{bmatrix}\varepsilon_x & \varepsilon_y & \varepsilon_z & \varepsilon_{yz} & \varepsilon_{zx} & \varepsilon_{xy}\end{bmatrix}^T \quad (10)$$

The matrix of elastic constants becomes:

Now, in the case of any constraint state, the elastic deformations are related to the constraints by the general Hooke law [20]:

So: $[\varepsilon_{el}]=[C]^{-1}\{\sigma\}$

The complete Hooke's law (valid in the thermoelastic deformations case) is then written:

$$\{\varepsilon_{tot}\}=\{\varepsilon_{th}\}+[C]^{-1}\{\sigma\} \quad (11)$$

$$\begin{cases} \varepsilon_x = a\Delta T + \dfrac{1}{E}(\sigma_x - v(\sigma_y+\sigma_z)) \;; & \varepsilon_{xy} = \dfrac{1+v}{E}\sigma_{xy} \\ \varepsilon_y = a\Delta T + \dfrac{1}{E}(\sigma_y - v(\sigma_x+\sigma_z)); & \varepsilon_{yz} = \dfrac{1+v}{E}\sigma_{yz} \\ \varepsilon_z = a\Delta T + \dfrac{1}{E}(\sigma_z - v(\sigma_y+\sigma_x)) \;; & \varepsilon_{xz} = \dfrac{1+v}{E}\sigma_{xz} \end{cases} \quad (12)$$

$a=\left(\dfrac{\partial\varepsilon}{\partial T}\right)_\sigma$ is the coefficient of linear thermal expansion and ΔT corresponds to the change of temperature. Hooke's law also allows to evaluate the stresses from deformations:

$$\begin{cases} \sigma_x = \dfrac{E}{h}\left[(1-v^2)(\varepsilon_x - a\Delta T) + (v+v^2) + (\varepsilon_y + \varepsilon_z + 2a\Delta T)\right.; \\ \sigma_y = \dfrac{E}{h}\left[(1-v^2)(\varepsilon_y - a\Delta T) + (v+v^2) + (\varepsilon_x + \varepsilon_z + 2a\Delta T)\right.; \\ \sigma_z = \dfrac{E}{h}\left[(1-v^2)(\varepsilon_z - a\Delta T) + (v+v^2) + (\varepsilon_x + \varepsilon_y + 2a\Delta T)\right.; \end{cases} \tag{13}$$

$$\left\{\sigma_{xy} = G_{xy}\varepsilon_{xy}\ ;\ \ \sigma_{yz} = G_{xy}\varepsilon_{yz};\ \ \sigma_{xz} = G_{xz}\varepsilon_{xz}\right.$$

Where $G_{xy} = G_{yz} = G_{xz} = \dfrac{E}{2(1+v)}$, $h = -2v^3 + -3v^2 + 1$ (14)

Thermal stresses, sometimes referred to as "thermal stresses", come from the fact that a material subjected to a change in temperature is constrained in such a way that it cannot deform freely. In this case, the thermal deformation is compensated by elastic deformation. It is therefore the elastic deformation (which corresponds to a displacement of the atoms with respect to their equilibrium position, which has changed with temperature) which is at the origin of the stress, it is only indirectly that the temperature change induces a stress.

2.5 Elastic limit criteria

In a one-dimensional tensile test, the elastic limit is defined as the stress for which the first plastic deformations appear. Below this limit, all deformations generated during the loading of the specimen can be recovered. This definition of the elastic domain for an axial plain test must be generalized in the case of complex loading. This three-dimensional generalization is called the plasticity criterion. It allows to define. In the space of the stresses, the region for which the material will have an elastic behavior. The definition of the two most widely used isotropic criteria for metals, the Tresca and Von Mises criteria is given below.

2.5.1 Criterion of Tresca

The maximum shear stresses are given by the expressions:

$$\begin{cases} \tau_{max12} = \frac{1}{2}(\sigma_{p1} - \sigma_{p2}) \\ \tau_{max13} = \frac{1}{2}(\sigma_{p1} - \sigma_{p3}) \\ \tau_{max23} = \frac{1}{2}(\sigma_{p2} - \sigma_{p3}) \end{cases} \tag{15}$$

Where: τ_{max} Maximum shear stress and σ_p Main stress.

The material must meet the following strength requirements:

$$\sigma_{max} \leq [\sigma]_{adm} \quad \text{and} \quad \tau_{max} \leq \frac{[\sigma]_{adm}}{2} \tag{16}$$

Where: σ_{adm} allowable stress

2.5.2 Criterion of Von Mises

There exists another criterion to check the resistance condition, it is the one given by Von-Mises, it defines the equivalent stress by:

$$\sigma_e = \sqrt{\frac{1}{2}[(\sigma_{p1} - \sigma_{p2})^2 + (\sigma_{p1} - \sigma_{p3})^2 + (\sigma_{p3} - \sigma_{p2})^2]} \tag{18}$$

The material must meet the following strength requirement: $\sigma_e \leq [\sigma]_{adm}$, where σ_e is an equivalent stress.

3 RESULTS AND DISCUSSION

Among the obtained results, we shows on the (Fig.2) and (fig.3) respectively the mesh of combustion chamber and boundary layer at the outlet wall of the combustion chamber realized by Ansys workbench software, we note here that the Inflation layer thickness should be defined to capture the boundary layer. This depends upon the flow characteristics and will need to be evaluated on a case by case basis.

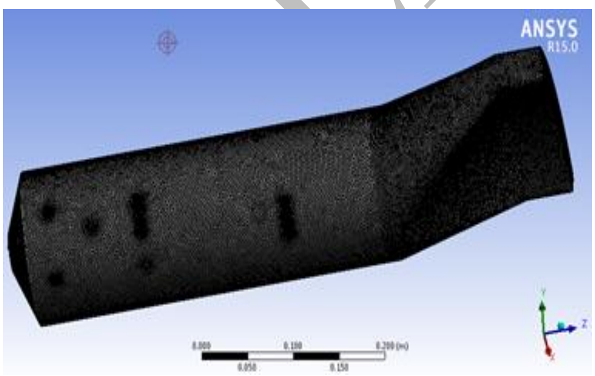

Fig. 2. Mesh of combustion chamber Of the Allison T56 engine

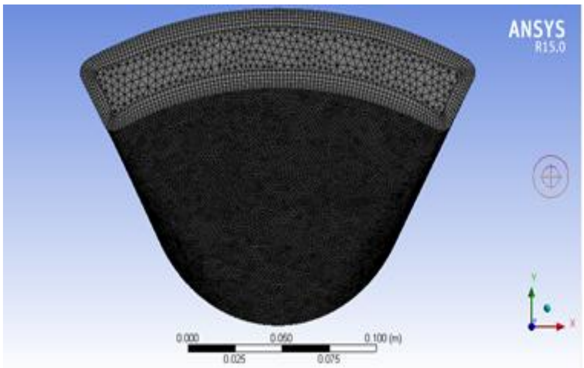

Fig.3 Mesh and boundary layer at the outlet wall of the combustion chamber

We observe on the figure 4 the iso-temperature map in the combustion chamber. The distribution of the temperature in the combustion chamber reaches a maximum of 2130 K at the end of the primary reaction zone (Fig.4) and (fig.5) , Air are provided by the primary holes to support the flame and a recirculation flow is produced in the primary zone due to the impact of the primary jets on the fuel flow, it ensures that some of the fuel can pass with the direction of the flow to be mixed with inlet air; Hence increase the air / fuel flow and consequently the combustion temperature increases. We can easily see that the symmetry of the flame formed is quite good.

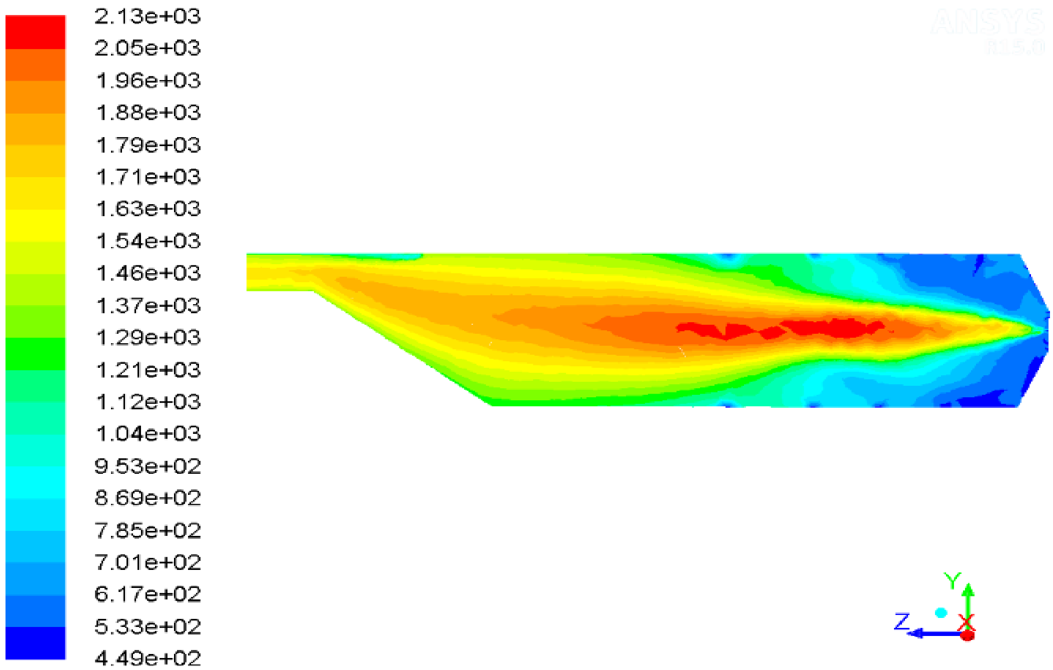

Fig.4. Simulation of turbulent flame in the combustion chamber (iso-total temperature map)

Figure 5 illustrates the influence of the preheating temperature of the air / fuel mixture on the combustion temperature along the combustion chamber. Concerning the maximum temperature, it is noted that the increase in the inlet temperature raises the maximum temperature, thus for a preheating temperature of 450 K; The Max temperature is of the order of 2050k, whereas for an input temperature of 566k, the Tmax = 2280k. As well as for that of the outlet by increasing the inlet temperature, the outlet temperature varies from 1210 K to 1420 K. This allowed us to conclude that the preheating of the air / fuel mixture improves combustion efficiency.

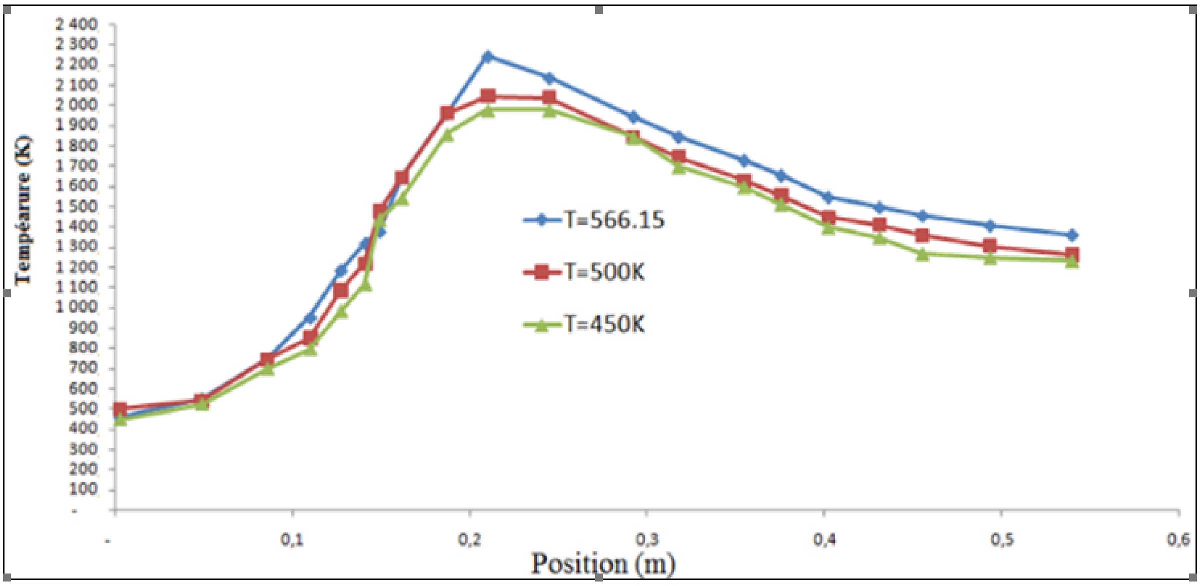

Fig.5. Distribution of the temperature in the combustion chamber as a function of the preheating temperature

The figure 6 presents pathline colored by total temperature, it is clear that at the exit of the combustion chamber the temperature reaches the TIT (Turbine inlet temperature) limited by the manufacturer [9,22-23].

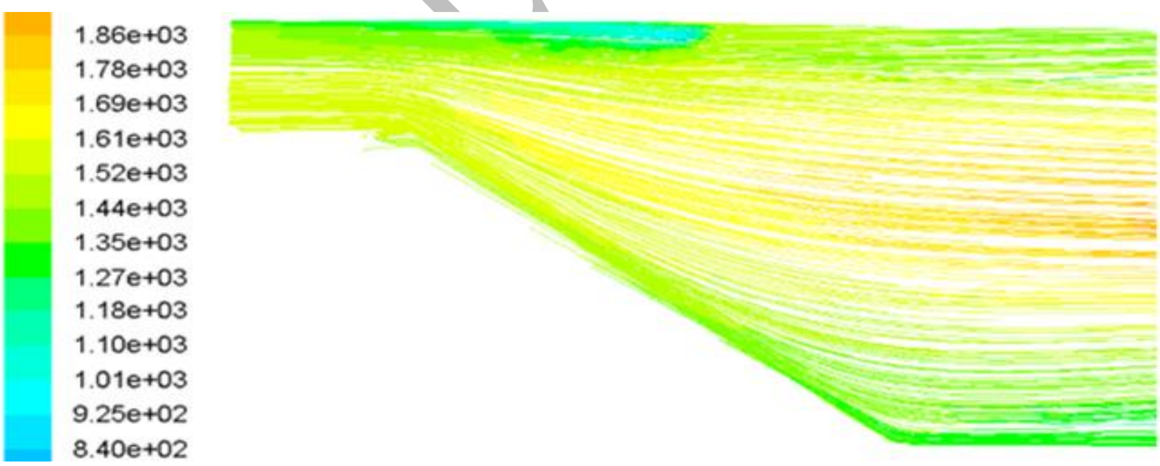

Fig.6. Pathline colored by total temperature [k]

Figure 7 presents the contours of turbine inlet temperature (TIT) for the non symetrical dilution holes positions at the outlet combustion chamber (real case) [k]. We notice that the temperature TIT is low at the wall because of the flow of dulition, and it is maximum in the center of the exit section of the chamber, but there is a decymetry in the distrubituion of the temperature because a non-symmetrical positions of the dilution holes. Consequently, we propose in figure 8 a possible modification of the dilution holes position, so that the hot flow at the outlet of the combustion chamber is symmetrical and consequently improves the distribution of thermal stresses at the wall, the efficiency and the life time of the combustion chamber and turbine. The numerical exit temperature distribution (TIT) is validated by the experimental results shown on the figure 13 realized on the turboprop engine Allison-T56 test bench of Air-Algerie company and is within an error of less than 9 percent.

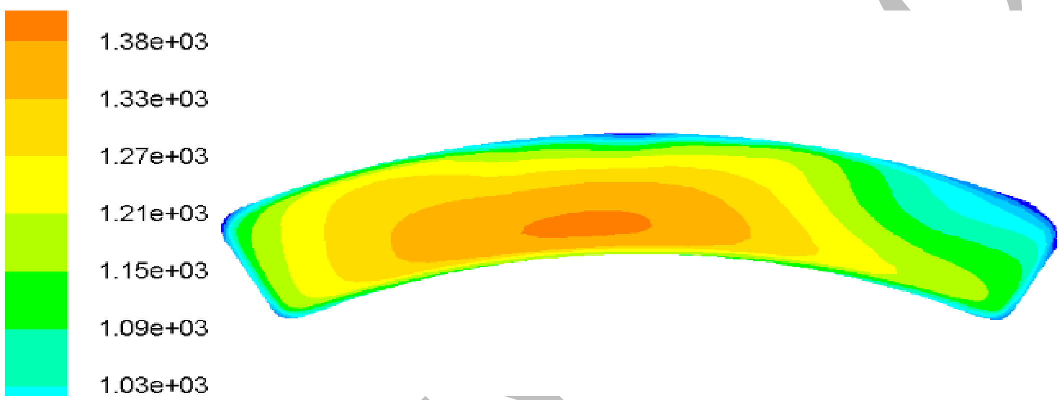

Fig.7. Contours of turbine inlet temperature (TIT) for the non symetrical dilution holes positions at the outlet combustion chamber (real case) [k].

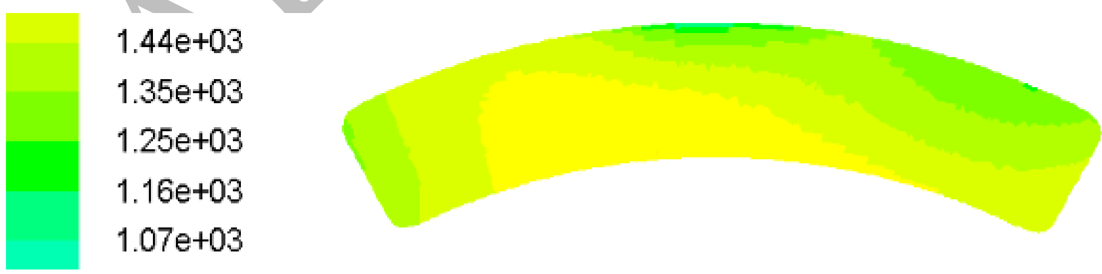

Fig.8. Contours of turbine inlet temperature (TIT) for the symetrical dilution holes positions at the outlet combustion chamber (possible modification-proposed case) [k]

Figure 9 depict a frontal view of the temperature distribution on the wall of the dome, at the operating conditions specified in table 1. In this figure we introduced the cartisian velocities components of flow instead of the axial flow according to the boundary conditions specified on the table 2, and this in order to create a film of air, which embraces and protects the internal wall of the dome, against the thermal stresses caused by the dynamic combustion loads and the proporable backfire which degrades the structure of the dome see figure 10 ref [26]. Note that the simulated wall temperature of the dome is much lower than the maximum temperature of the combustor material where the maximum allowable temperature for Hastelloy-X (material of the combustor) is approximately 1175k [25].

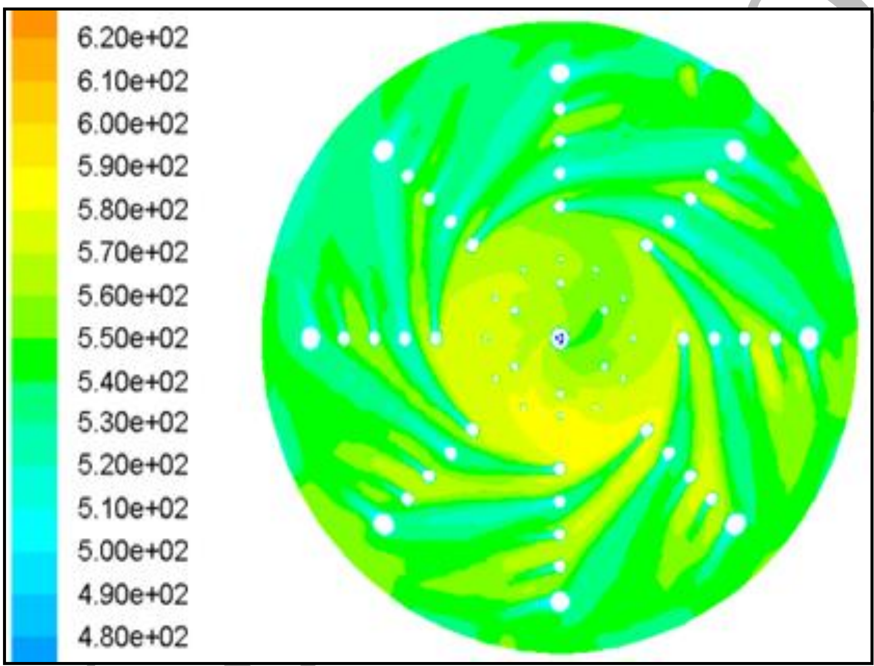

Fig.9. Dome wall temperature and exit temperature distribution

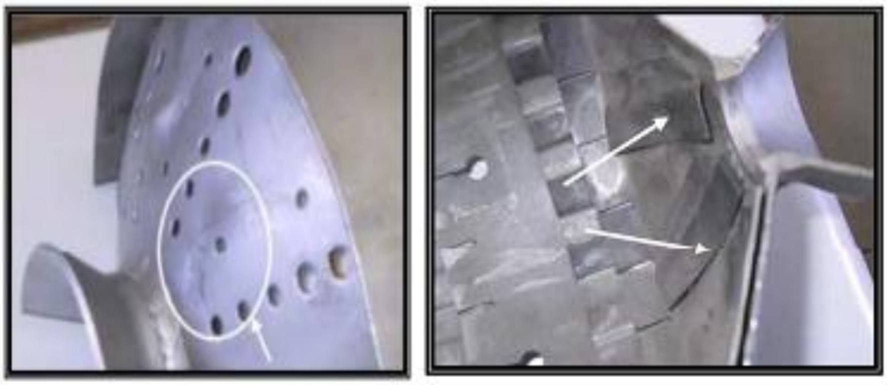

Fig.10. Defects on combustor dome [26] ; (a) Crack formation on dome wall, b(Thermal distortion of the splash cooling devices on the inside of the dome

Figure 11 depicts, the vectors velocity variation of the internal flow field according to the boundary conditions of Table 1 and 2. It is apparent that the flow field is in the form of a cyclone which embraces the internal wall of the dome.

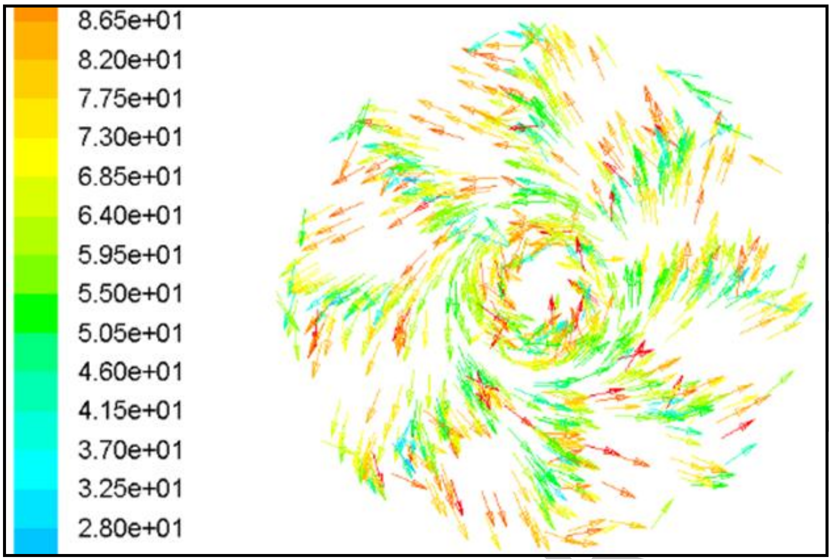

Fig.11. Velocity vectors colored by velocity magnitude at the dome section [feet/s]

Figure 12 depicts, the variation of the velocity victors of the internal flow through the combustion chamber, it can be seen the weak recirculation zone due to the quite high speed of flow at the level of the injector, which allows the fuel droplets to mix with the oxidizer but at the level of the walls, the velocity of the fluid mixture is relatively low because of the pressure drops. The mixture (fuel-air) in the core of the combustion chamber passes through the primary combustion zone without taking part in the recirculation zone. The recirculation

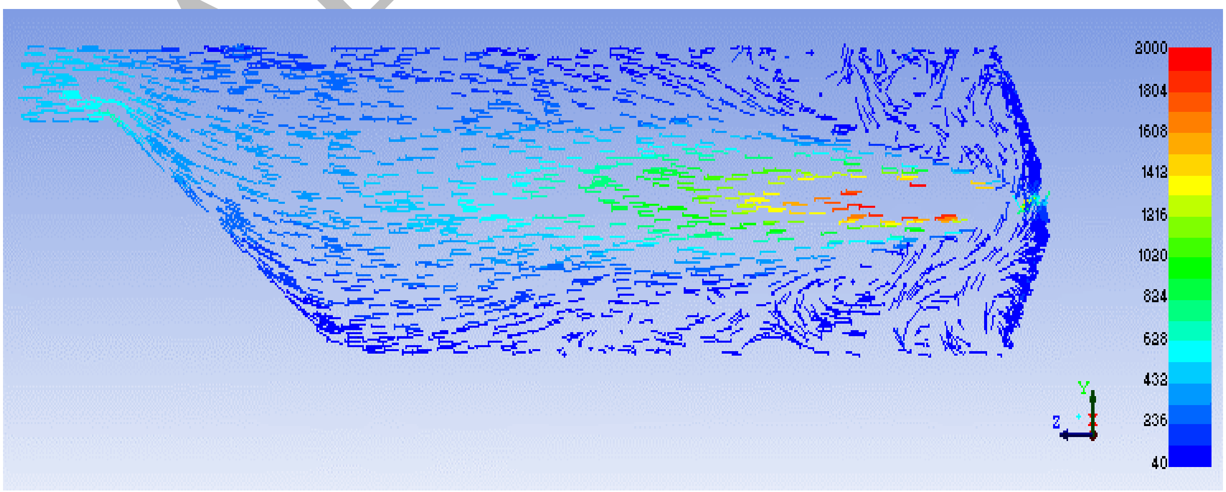

Fig.12. Velocity vectors through the combustion chamber [feet/s]

zone is weak and is situated too far downstream from the dome, thereafter, the flow becomes more stable in the dilution zone where the combustion gases are cooled before reaching the outlet of the combustion chamber. At the outlet of the combustor the ejection velocity is of the order of 600 [feet/s].

Fig.13 depicts the variation of the turbine inlet temperature TIT as a function of fuel flow, it is noted that the variation of the TIT is proportional with the fuel flow, on the other hand the figure presents two curves, the first is the result of the simulation by the Ansys-fluent software, and the second is an experimental result obtained on the Air-Algerie turboprop test-bench, it is clear that the two results coroborate each other with a relative difference of less than 9%, in addition the experimental results serve as validation to previous numerical results. We can conclude that fuel flow is the most important factor in combustion because it is the only parameter that can be controlled manually through a throttle, also it ensures the control of the TIT and consequently the performance of the engine.

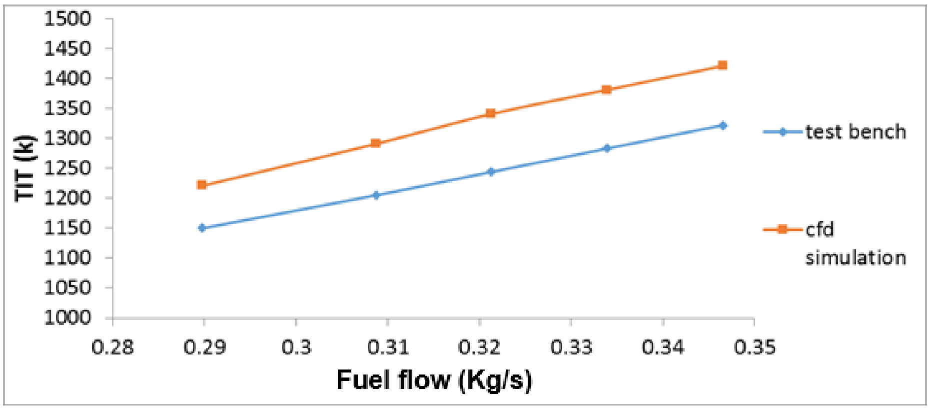

Fig.13. Influence of fuel flow variation on the TIT (turbine inlet temprerature)

Figure 14 and figure 15 depict respectively, the variation of the equivalent stress with Von-Mises criterion and the variation of the maximum main stress using Ansys-fluent-Structure software, according to the physical characteristic of the combustor material (Hastelloy-X) specified on the table 3. We note that both the equivalent stress and the maximum main stress follow the same behavior as the temperature through the combustion chamber (figures 4 & 5), so they start to increase in the primary zone of the combustor until they reach a maximum and then they gradually decrease in the secondary zone of the chamber where the temperature stabilizes at the TIT.

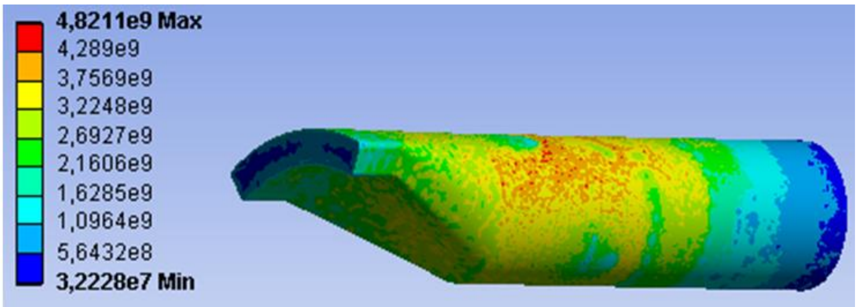

Fig.14. Variation of the equivalent stress with Von-Mises criterion

Table 3. Main physical characteristic of the combustor material (Hastelloy-X) given by Ansys fluent data base and ref [25]

Physical propriety	**value**
Volumic masse [kg/m^3]	8874
Yong moduls [MPa]	2e+05
Poisson coefficient	0.3
Compressibility modulus [Pa]	1.6667E+11
Shear modulus [Pa]	7.6923e10
Isotrope thermic conductivity [Wm^{-1}k^{-1}]	16.9
Specific heat [J.kg^{-1}k^{-1}]	446
Fusion temperature [c]	1452.9

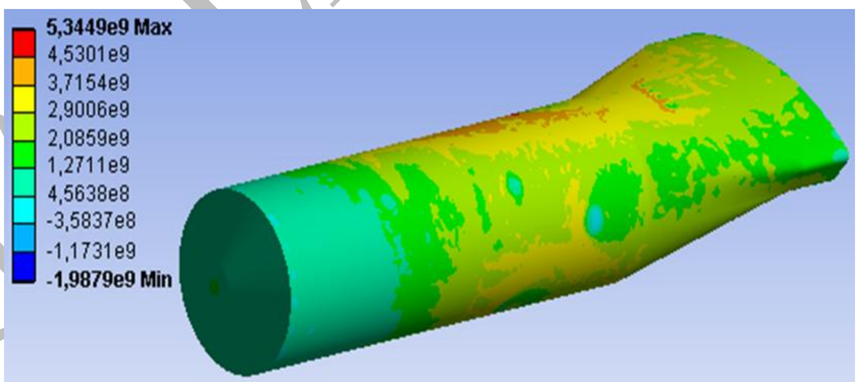

Fig.15. Maximum main stress

4. CONCLUSION

In this study devoted to the numerical simulation of the turbulent diffusion flame in the combustion chamber of the engine Allison T56, it has been realized the mesh of the rather complex geometry of the combustion chamber using Ansys –Fluent software, a sensitivity study is made for the choice of optimum mesh. Furthermore this study allowed us to see the influence of the injection gas temperature or preheating temperature on the flame structure. We can easily see that the symmetry of the flame formed is quite good, the temperature is maximum at the center which is logical and the turbine inlet temperature (TIT) is between 1200 and 1400 k. This allowed us to conclude that the preheating of the air / fuel mixture improves combustion efficiency. On the other hand, there is a decymetry in the distrubituion of the TIT (fig.7) because a non-symmetrical positions of the dilution holes. Consequently, we propose in figure 8 a possible modification of the dilution holes position, so that the hot flow at the outlet of the combustion chamber is symmetrical and consequently improves the distribution of thermal stresses at the wall, the efficiency and more life time of the combustion chamber and turbine. Another possibility of modification can be applied to the dome of Allison T56 combustion chamber, it concerns the introduction of the cartisian velocities components of flow instead of the axial flow in order to create a film of air, which embraces and protects the internal wall of the dome, against the thermal stresses caused by the dynamic combustion loads and the proporable backfire which degrades the structure of the dome.

The numerical exit temperature distribution (TIT) is validated by the experimental results shown on the figure 13 realized on the turboprop engine Allison-T56 test bench of Air-Algerie company and is within an error of less than 9 percent. Furthermore, the variation of the equivalent stress with Von-Mises criterion and the variation of the maximum main stress for the same Hastelloy-X (material of the combustor) follow the same behavior as the temperature through the combustion chamber. It is concluded that the thermal stresses are highest for high temperatures and become minimum for low temperatures.

5. REFERENCES

[1] R.Borghi, P.Clavin, A.Linan,P.Pelcé & G.I.Sivashinsky, Modélisation des phénomènes de combustion, Paris 1985.

[2] R.Rebeh , M.Alliche et M.Mamou, Validation des modèles de turbulence pour la simulation des écoulements turbulents de l’air autour d’un obstacle à section carrée, Second International Conférence on Applied Energetics and Pollution, 2014 Algerie.

[3] Jean-Pierre SAWERYSYN, « la combustion du bois et ses impacts sur la qualité de l’air » Air Pur - N°81, Lille France,2012.

[4] R.RENANE «Caractérisation et modélisation d’une chambre de combustion tubulaire sous l’influence des charges dynamique et de combustion » Thèse de doctorat, UMBB Algerie 2013.

[5] Yves D'Angelo, « Analyse et simulation numérique de phénomènes liés à la combustion supersonique », Thèse, ENPC France, 1994.

[6] Matthieu Rullaud, « modélisation de la combustion turbulente via une méthode de tabulation de la cinétique chimique détaillée couplée à des fonctions densités de probabilité. Application aux foyers aéronautiques » Thèse, INSA de Rouen France 2004.

[7] Lars Davidson, « An Introduction to Turbulence Models », Chalmers University Of Technology, Goteborg, Sweden, November 2003.

[8] F.W. Skidmore, D.R. Hunt, P.N. Doogood, “The reduction of smoke emissions from allison t56 engine “, Propulsion Report 182, AUSITALIA, Mars 1990.

[9] Douvi C. Eleni, Tsavalos I. Athanasios and Margaris P. Dionissios, ” Evaluation of the turbulence models for the simulation of the flow over a National Advisory Committee for Aeronautics (NACA) 0012 airfoil”, Journal of Mechanical Engineering Research Vol. 4(3), pp. 100-111, March 2012, DOI: 10.5897/JMER11.074.

[10] John H.Lienhard IV, John H.Lienhard V, A Heat transfer textbook, third ed, Cambridge U.S.A 2001.

[11] Yogesh Jaluria, Kenneth E, Torrance, “Computational Heat transfer” ed Taylor & Francis, second edition, New York 2003.

[12] P.Amiot « Thermodynamique » Scientifique WorkPlace, Université de Laval, Canada 2006.

[13] Libuse Sykorova, Oldrich Suba, « The transient temperature field simulation of polymeric materials during Laser Machining », International Journal of Mechanics, Issue 3, Vol.5, 2011.

[14] Engine-Virtual-Training, https://www.behance.net/gallery/1643476/T56

[15] J.M Cros, Z.Q. Feng, Aéroélasticités (cours), Université d’Evry-Val d’Essonne, septembre 2009.

[16] Roland FORTUNIER, « Comportement Mécanique des Matériaux » Ecole Nationale Supérieure des Mines Saint-Etienne 2009.

[17] Manuelita BONADIES, «Thermoelastic stress analysis for linear thermoelastic bodies » Department of Mathematics, University of Turin, ITALY, Vol. 65, 2, 2007.

[18] W. D. KINGERY, Factors affecting thermal stress resistance of ceramic materials, Journal of the American ceramic society, Vol. 38, issue 1, 1955.

[19] Peigne, Philippe. Resistance aux chocs thermiques des ceramiques thermomecaniques. Thèse. Villeurbanne : Institut National des Sciences Appliquées de Lyon, 1991

[20] Jean salençon, Mécanique des Milieux Continus (Concept Généraux), Edition Ecole polytechniques, Palaiseau 2007.

[21] Nezih Mrad, Development of CFD capabilities in Xact life, Technical report, Life prediction technologies, Otawa Canada 2015.

[22] F.W.Skidmore, D.R. Hunt, P.N.Doogood « The reduction of smoke emissions from Allison T56 engine », Propulsion report 182, Aeronautical research laboratory, Royal Australian Air force, Melbourne, Vectoria, March 1990.

[23] F.W.Skidmore, “The influence of gas turbine combustor fluid mechanics on smoke emissions” , Thesis, Institute of thecnology Victoria, Australia, Dec 1988.

[24] Bredberg J., Peng S.H, Davidson L, “An improved k-ω turbulence model applied to recirculating flows”. International journal of Heat and Fluid Flow 23,6(2002),731-743.

[25] Warner Martiensser, Hans Warlimont “ Springer Handbook of condensed matter and matterials data, Springer, Frankfurt Sept 2004.

[26] Gouws J.J, Morris R.M and Visser J.A, “ Modelling of a gas turbine combustor using a network solver”, South African journal of science 102, Nov/Dec 2006.

How to cite this article:
Renane R, Allouche R, Laazab S, Nour A.Computations of turbulent non-premixed combustion and modeling of flame wall interaction. J. Fundam. Appl. Sci., 2019, *11(2), 605-622*.